Inorg. Chem. **2008**, *47*, 10491−10498

The Mn^{2+}−Bicarbonate Complex in a Frozen Solution Revisited by Pulse W-Band ENDOR

Alexey Potapov and Daniella Goldfarb*

Department of Chemical Physics, Weizmann Institute of Science, Rehovot 76100, Israel

Received June 18, 2008

The coordination of bicarbonate to Mn^{2+} is the simplest model system for the coordination of Mn^{2+} to carboxylate residues in a protein. Recently, the structure of such a complex has been investigated by means of X-band pulse EPR (electron paramagnetic resonance) experiments (Dasgupta, J.; et al. *J. Phys. Chem. B* 2006, *110*, 5099). Based on the EPR results, together with electrochemical titrations, it has been concluded that the Mn^{2+} bicarbonate complex consists of two bicarbonate ligands, one of which is monodentate and other bidentate, but only the latter has been observed by the pulsed EPR techniques. The X-band measurements, however, suffer several drawbacks. (i) The zero-field splitting (ZFS) term of the spin Hamiltonian affects the nuclear frequencies. (ii) There are significant contributions from ENDOR (electron nuclear double resonance) lines of the $M_S \neq \pm 1/2$ manifolds. (iii) There are overlapping signals of ^{23}Na. All these reduce the uniqueness of the data interpretation. Here we present a high-field ENDOR investigation of $Mn^{2+}/NaH^{13}CO_3$ in a water/methanol solution that eliminates the above difficulties. Both Davies and Mims ENDOR measurements were carried out. The spectra show that a couple of slightly inequivalent ^{13}C nuclei are present, with isotropic and anisotropic hyperfine couplings of $A_{iso1} = 1.2$ MHz, $T_{\perp 1} = 0.7$ MHz, $A_{iso2} = 1.0$ MHz, $T_{\perp 2} = 0.6$ MHz, respectively. The sign of the hyperfine coupling was determined by variable mixing time (VMT) ENDOR measurements. These rather close hyperfine parameters suggest that there are either two distinct, slightly different, carbonate ligands or that there is some distribution in conformation in only one ligand. The distances extracted from $T_{\perp 1}$ and $T_{\perp 2}$ are consistent with a monodentate binding mode. The monodentate binding mode and the presence of two ligands were further supported by DFT calculations and ^1H ENDOR measurements. Additionally, ^{23}Na ENDOR resolved at least two types of $^{23}Na^+$ in the Mn^{2+}−bicarbonate complex, thus suggesting that the bicarbonate bridges two positively charged metal ions.

1. Introduction

The divalent Mn^{2+} ion plays an essential role in many biological processes; furthermore, it can be used as a paramagnetic probe, substituting for other divalent metal ions in enzymatic reactions.[1] In particular, Mn^{2+} can replace Mg^{2+}, which is a major cofactor in many processes in the living cell. Such a substitution is possible owing to the fact that, despite some differences, the coordination geometry, the stability, and the ligand exchange rates are similar for both ions. These similarities make Mn^{2+} the least perturbing substitute of Mg^{2+} in enzymatic reactions.[1]

The main motivation for Mg^{2+} to Mn^{2+} replacement is to employ the latter as a paramagnetic reporter in active sites of enzymes[1] or ribozymes.[2] The hyperfine interactions of the unpaired electrons of Mn^{2+} with surrounding nuclei can be probed using electron−nuclear double resonance (ENDOR) spectroscopy. These interactions reflect details of the binding site geometry, and their analysis can ultimately lead to insights into the mechanism of the enzymatic reaction. One of the frequently found ligands to Mn^{2+} in proteins are carboxylate side chains, which can be identified through the ENDOR signals of ^{13}C-labeled proteins.

The approach of Mn^{2+} substitution and ^{13}C labeling has been recently applied in the investigation of the metal binding site in the wild-type Ras·GDP protein and its oncogenic mutant G12V using W-band (95 GHz) ENDOR experiment.[3] The ^{13}C ENDOR spectra of uniformly ^{13}C-labeled protein

* To whom correspondence should be addressed. E-mail: daniella.goldfarb@weizmann.ac.il.

(1) Reed, G.; Poyner, R. *Metal Ions Biol. Syst.* **2000**, *37*, 183–207.

(2) Morrissey, S.; Horton, T.; Grant, C.; Hoogstraten, C.; Britt, R.; DeRose, V. *J. Am. Chem. Soc.* **1999**, *121*, 9215–9218.

10.1021/ic8011316 CCC: $40.75
Published on Web 10/24/2008

complexes with several nucleotides identified the interactions of Ser17 and Thr35 residues with the Mn^{2+} ion. The isotropic hyperfine couplings, A_{iso}, were in the range of 0.46−1.0 MHz, and the anisotropic hyperfine interaction could be accurately described by the point dipole−dipole interaction giving Mn−C distances from 3.1 to 3.4 Å. Interestingly, the absence of a large number of overlapping species and signals from background nuclei allowed determining the sign of A_{iso} from the line shape of the spectrum. Density functional theory (DFT) calculations were carried out as well and predicted hyperfine couplings with magnitude and sign close to the experimental values. The ENDOR spectrum of the protein labeled with 1,4-^{13}C-aspartate did not show any ^{13}C signals, thus ruling out the hypothesis that Asp57 is coordinated to the Mn^{2+} ion; namely, carboxylate coordination has not been detected.

For the purpose of identifying Mn^{2+} binding to carboxylate residues and for understanding its coordination mode in protein active sites, we have chosen the Mn^{2+}−carbonate complex as the simplest possible model. This complex has been already studied by means of X-band (9.5 GHz) pulsed EPR techniques with an outlook for the investigation of the water oxidizing complex in photosystem II.[4,5] On the basis of the analysis of X-band ^{13}C ESEEM (electron spin echo envelope modulation), HYSCORE (hyperfine-sublevel correlation spectroscopy) and ENDOR, combined with electrochemical titrations, Dasgupta et al. proposed that two carbonates are coordinated to the metal ion: one in a bidentate mode and the other in a monodentate mode. The ^{13}C signal of the bidentate ligand was observed experimentally, while that of the monodentate ligand was inferred indirectly. The spectral analysis was complicated because of the following three reasons. First, the Mn^{2+} ion is a high-spin ion ($S = {}^5/_2$), the electron spin transitions of which overlap severely at X-band, and therefore ENDOR and HYSCORE spectra contain contributions from electron spin manifolds other than $M_S = \pm{}^1/_2$ and they cannot be ignored.[6−8] Second, at X-band frequencies the zero-field splitting (ZFS) term has significant contributions to the nuclear frequencies and the transition probabilities.[9,10] Consequently, it should be included in the simulation of ESEEM, HYSCORE, and ENDOR spectra. This increases considerably the number of unknown parameters (ZFS and hyperfine tensors, strains, etc.) and therefore reduces the uniqueness of the parameters found in simulations. The third reason is the overlap of ^{23}Na and ^{13}C signals. Isolation of the ^{13}C signals requires subtraction of spectra of samples with ^{13}C-labeled and nonlabeled bicarbonate. These problems become negligible once the measurements are carried out at a high frequency, such as W-band (95 GHz), because the electron spin Zeeman interaction term is much larger than the ZFS term and therefore the latter does not affect the ENDOR frequencies. Moreover, the central electron spin transitions, $|-{}^1/_2,m_I\rangle \leftrightarrow |-{}^1/_2,m_I\rangle$, are intense and narrow and comprise the major contribution to the echo,[11] and the nuclear frequencies of ^{13}C and ^{23}Na are well separated.

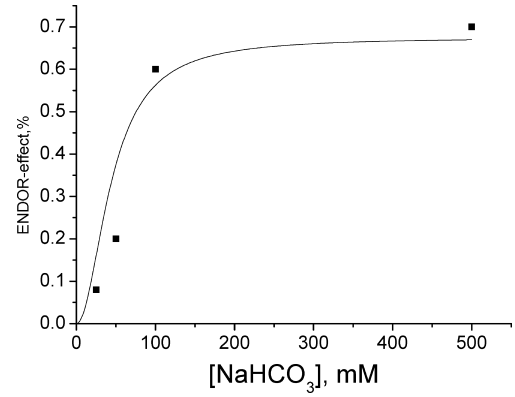

Figure 1. Dependence of the ^{13}C Mims ENDOR effect on [$NaH^{13}CO_3$]. The solid line was calculated from the binding constants given in preceding work for [Mn^{2+}] = 0.5 mM.[4]

In this work, we present pulse W-band ENDOR measurements on the Mn^{2+} ^{13}C-enriched bicarbonate complex. The spectra reveal two types of ^{13}C nuclei with slightly different hyperfine couplings which were interpreted in terms of Mn−^{13}C distances, showing that the carbonate ligand is monodentate. This conclusion was further corroborated by DFT (density functional theory) calculations that together with ^{1}H ENDOR and earlier electrochemical titrations[4] show that there are two carbonate ligands. In addition, distant and proximal ^{23}Na ions were resolved in the ENDOR spectra, confirming the expected presence of complexes with carbonate ligands bridging Mn^{2+} and Na^+ cations.

2. Experimental Section

Sample Preparation. The complex of Mn^{2+} and bicarbonate was prepared by mixing a solution of $MnCl_2$ with varying amounts of $NaH^{13}CO_3$ (Cambridge Isotopes) self-buffering at pH 8.3. For a good glass formation upon freezing, methanol was added in 1:1 ratio by volume. The complex is stable for several minutes; afterward a brownish precipitate of $MnCO_3$ is formed. Therefore, after mixing the components, quartz capillaries were rapidly filled and the solution was frozen by immersing the samples into liquid nitrogen before precipitation takes place. Afterward, the samples were mounted into the EPR probehead that was placed into the precooled cryostat at 10 K. The formation of the complex has been tested by titrations with $NaH^{13}CO_3$. Since the ENDOR line shape does not vary with concentration, the ENDOR-effect can be used as a measure of the complex amount. Here, the normalized intensity of the ^{13}C ENDOR (referred to as ENDOR efficiency, see below) was measured as a function of [$NaH^{13}CO_3$], as shown in Figure 1. The data were fitted with an equilibrium constant $K = 550\ M^{-2}$

(3) Bennati, M.; Hertel, M.; Fritscher, J.; Prisner, T.; Weiden, N.; Hofweber, R.; Sporner, M.; Horn, G.; Kalbitzer, H. *Biochemistry* **2006**, *45*, 42–50.
(4) Dasgupta, J.; Tyryshkin, A.; Kozlov, Y.; Klimov, V.; Dismukes, G. *J. Phys. Chem. B* **2006**, *110*, 5099–5111.
(5) Dasgupta, J.; Tyryshkin, A. M.; Dismukes, G. C. *Angew. Chem.* **2007**, *46*, 8028–8031.
(6) Tan, X.; Bernardo, M.; Thomann, H.; Scholes, C. P. *J. Chem. Phys.* **1993**, *98*, 5147–5157.
(7) Coffino, A. R.; Peisach, J. *J. Chem. Phys.* **1992**, *97*, 3072–3091.
(8) Benetis, P.; Dave, N.; C, P.; Goldfarb, D. *J. Magn. Reson.* **2002**, *158*, 126–142.
(9) Vardi, R.; Bernardo, M.; Thomann, H.; Strohmaier, K. G.; Vaughan, D. E. W.; Goldfarb, D. *J. Magn. Reson.* **1997**, *126*, 229–241.
(10) Astashkin, A. V.; Raitsimring, A. M. *J. Chem. Phys.* **2002**, *117*, 6121–6132.
(11) Manikandan, P.; Carmieli, R.; Shane, T.; Kalb (Gilboa), A. *J. Am. Chem. Soc.* **2000**, *122*, 3488.

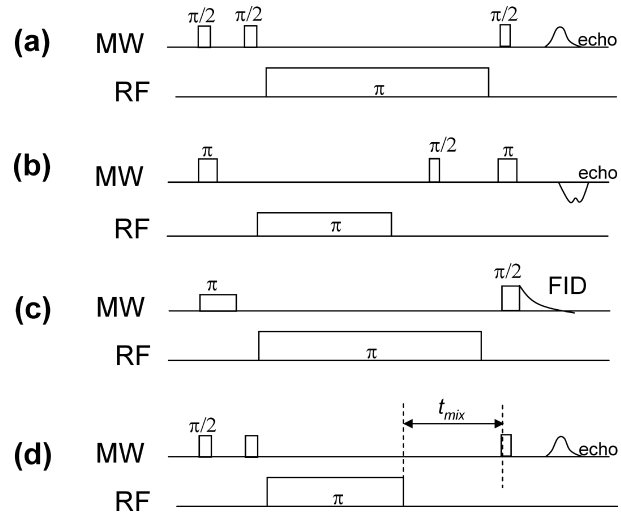

Figure 2. Pulse sequences used in this work: (a) Mims ENDOR, (b) Davies ENDOR with echo detection, (c) Davies ENDOR with a long inversion pulse and FID detection, and (d) VMT Mims ENDOR with a long mixing interval after rf pulse.

determined earlier.[4] The same preparation procedure was used for the preparation of the Mn^{2+}−carbonate complex.

Spectroscopic Measurements. ENDOR measurements were carried out on a home-built W-band spectrometer operating at 94.9 GHz[12] with an upgraded MW bridge.[13] Measurements were performed with the magnetic field set to one of the hyperfine components of the central transition $|-^1/_2,m_I\rangle \leftrightarrow |^1/_2,m_I\rangle$, where m_I corresponds to projection of the nuclear spin of ^{55}Mn. In our particular case, the line corresponding to $m_I = {}^3/_2$ was chosen. Neglecting effects of the ZFS term, the population difference of the central transition for a system with a total spin $S = k/2$ is given by

$$P = \frac{e^{g_e\beta_e B_0/2kT} - e^{-g_e\beta_e B_0/2kT}}{\sum_{m=-k/2}^{k/2} e^{m(g_e\beta_e B_0/kT)}} = \frac{(1-e^{\beta})(1-e^{-\beta})}{e^{-\beta(k+1)/2} - e^{\beta(k+1)/2}} \quad (1)$$

where $\beta = g_e\beta_e B_0/kT$. For $S = {}^5/_2$, the value of β that maximizes P is ∼0.67. For electron spin with $g_e = 2$ at $B_0 = 3.3$ T the Zeeman temperature is 4.4 K, and this optimal polarization is achieved at 6.5 K. However, at 10 K the spin−lattice relaxation time (T_1) affords a faster repetition rate of 200 Hz, thus compensating for the loss in signal-to-noise ratio caused by the smaller polarization. Accordingly, the measurement temperature we chose was 10 K.

ENDOR spectra were measured using the Mims ENDOR sequence (Figure 2a) and Davies ENDOR pulse sequence with an echo or FID detection (Figure 2b,c). The sign of the hyperfine coupling was determined by the variable mixing time (VMT) Mims ENDOR sequence (Figure 2d),[14,15] which is similar to the Mims ENDOR sequence, but with an additional delay, t_{mix}, inserted after the RF (radio frequency) pulse. The random acquisition method was applied for all ENDOR measurements.[16] The experimental parameters are given in the figure captions and the text.

The length of the RF π pulse was determined by a ^{1}H Rabi-nutation experiment on a BDPA (α,γ-bisdiphenylene−β-phenyl allyl in polyethylene) sample. Based on the result for ^{1}H, the length of π pulse for ^{13}C was calculated by scaling the ^{1}H π pulse by the appropriate γ ratio and taking into account the frequency dependence of the rf power. This yielded a π pulse of 30 μs for ^{13}C. Though not optimal, for simplicity the same length has been used to record the ^{23}Na spectrum.

Spectral Simulations. The ground state of the Mn^{2+} ion is ^{6}S. Since the orbital moment is equal to zero, and the slightly distorted octahedral crystal field is weak, the unpaired electron has an isotropic g value and a relatively small zero-field splitting.[17] The spin Hamiltonian can be written as

$$\hat{H} = g_e\beta_e\vec{B}_0\hat{S} + \hat{S}\mathbf{D}\hat{S} + \sum_i (\hat{S}\mathbf{A}\hat{I}_i - g_n\beta_n\vec{B}_0\hat{I}_i + \hat{I}_i\mathbf{P}\hat{I}_i) \quad (2)$$

The first term here represents the Zeeman interaction of an unpaired electron with the external magnetic field, the second represents the zero-field splitting, the third represents hyperfine interaction of the electron with a magnetic nucleus, and finally fourth and fifth stand for nuclear Zeeman and quadrupolar interactions. The summation is performed over all the nuclei coupled to the electron spin. In the first order of perturbation theory, the last two terms do not contribute to the EPR spectrum. While for the ^{55}Mn nucleus the hyperfine interaction is large and does contribute to the EPR spectrum, for the other nuclei it is not resolved and contributes only to the broadening of the EPR line. The zero-field splitting term results in a tilt of the quantization axis of the electron spin; similarly the anisotropic hyperfine and quadrupolar interactions tilt the quantization axis of a nuclear spin. The criterion for the magnetic field at which the effects of the tilted axis can be ignored is

$$g_e\beta_e B_0 \gg D_{||}, \quad g_n\beta_n B_0 \gg T_{||}, P_{||} \quad (3)$$

where $D_{||}$, $T_{||}$ and $P_{||}$ are the largest values of the ZFS, anisotropic hyperfine and nuclear quadrupole interaction. As will be demonstrated later, those conditions are mutually fulfilled for the ligand nuclei of the Mn^{2+}−carbonate complex at the W-band. Under these conditions, the ENDOR frequencies corresponding to nuclear transitions $m_I \leftrightarrow m_I - 1$ are determined only by the last three terms and given to first order by

$$\nu_{Ms}(M_I) = |-\nu_L + M_S A + P(2m_I - 1)| \quad (4)$$

where ν_{Ms} is the ENDOR frequency within a particular M_S manifold, ν_I is the Larmor frequency of the nucleus, and P and A are the relevant angular dependent components of nuclear quadrupolar and hyperfine tensors, respectively. ENDOR spectra do not depend on other parameters and therefore the analysis of spectra is relatively simple.

The ENDOR effect is defined as

$$E = \frac{I(\mathrm{RF\,off}) - I(\mathrm{RF\,on})}{I(\mathrm{RF\,off})} \quad (5)$$

where I(RF on) and I(RF off) are the intensities of the signal with and without the application of the RF pulse.

Pulse ENDOR spectra are notorious for the presence of blind spots at the spectral region corresponding to small hyperfine couplings. Such a behavior is characteristic for all ENDOR sequences involving polarization transfer. To account for the blind

(12) Gromov, I.; Krymov, V.; Manikandan, P.; Arieli, D.; Goldfarb, D. *J. Magn. Reson.* **1999**, *139*, 8–17.
(13) Goldfarb, D.; Lipkin, Y.; Potapov, A.; Gorodetsky, Y.; Raitsimring, A.; Epel, B.; Radoul, M.; Kaminker, I. *J. Magn. Reson.* **2008**, *194*, 8–15.
(14) Epel, B.; Pöppl, A.; Manikandan, P.; Vega, S.; Goldfarb, D. *J. Magn. Reson.* **2001**, *148*, 388–397.
(15) Bennebroek, M. T.; Schmidt, J. *J. Magn. Reson.* **1997**, *128*, 199–206.
(16) Epel, B.; Arieli, D.; Baute, D.; Goldfarb, D. *J. Magn. Reson.* **2003**, *164*, 78–83.
(17) Abragam, A.; Bleaney, B. *Electron Paramagnetic Resonance of Transition Ions*; Clarendon Press: Oxford, UK, 1970.

spots, the spectra, simulated using the Matlab Easyspin package,[18] were multiplied by functions which model the experimental settings. The Mims ENDOR effect, E is modified by[19]

$$E \propto 1 - \cos(A\tau) \tag{6}$$

where A is the hyperfine coupling and τ is the interval between the first and the second pulses in the sequence. For echo-detected Davies ENDOR the function is[20]

$$E \propto \frac{(At_p)^2}{\frac{1}{2} + (At_p)^2} \tag{7}$$

where t_p is the length of the first inversion pulse. The suppression hole for FID-detected Davies experiment was calculated from the Bloch equations as described in the Supporting Information.

DFT Calculations. The geometry optimization was performed using Gaussian98[21] package at B3LYP level of theory using LanL2DZ basis set, which includes effective core potential for the Mn atom. The effects of solvent were accounted by the COSMO model. The resulting geometry was used as an input for the ORCA program,[22] performing the computation of the EPR parameters at a single point. These calculations employed hybrid B3LYP functional and the Ahlrichs TZV[23] basis with polarization functions for all the atoms, except for Mn^{2+}. For Mn the triply polarized CP(PPP)[24] basis set with an appropriate integration grid was utilized. The CP basis is based on the TurboMole DZ basis developed by Ahlrichs and co-workers and obtained from the basis set library found at ftp.chemie.uni-karlsruhe.de/pub/basen. The polarization sets consisted of 2p functions according to Wachters[25] and a 1f function taken from the aforementioned Turbomole library.

3. Results

3.1. ENDOR Measurements. The field-swept echo-detected (FS-ED) EPR spectrum of a frozen solution formed by mixing 1:1000 Mn^{2+} and $NaHCO_3$ is presented in Figure 3. It exhibits an intense sextet of lines, with a splitting of ~90 G, arising from the hyperfine splitting of the ^{55}Mn ($I = {}^5/_2$) central transitions $|-{}^1/_2,m_I\rangle \leftrightarrow |{}^1/_2,m_I\rangle$. The sextet is superimposed on a broad background arising from transitions other than central transitions. The D value was estimated from the half-width to be ~40 mT by assuming that this width corresponds approximately to half the splitting of the $|\pm{}^3/_2\rangle \leftrightarrow |\pm{}^1/_2\rangle$ transitions that is $\sim 2D$.[26] The line width of the sharp sextet components is determined by second-order effects, which scale like $\sim D^2/g\beta B_0$. Therefore, at the W-band the central transition hyperfine components are well resolved whereas at the X-band they are considerably broader.

ENDOR measurements were performed at the magnetic field position marked with an arrow in Figure 3. At this field the major contribution to the echo is from $|-{}^1/_2,m_I\rangle \leftrightarrow |{}^1/_2,m_I\rangle$ $m_I = {}^3/_2$ transition and the ENDOR spectrum is

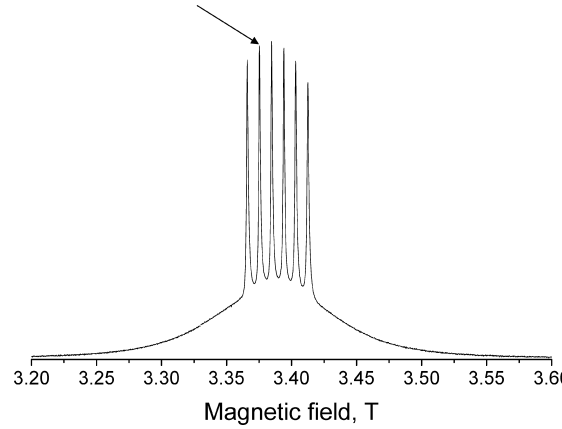

Figure 3. Field-swept echo-detected EPR spectrum of the Mn^{2+}−bicarbonate complex in a frozen solution, $[Mn^{2+}] = 0.5$ mM and $[NaHCO_3] = 500$ mM. The pulse sequence was $\pi/2-\tau-\pi-\tau-$echo, with $t_{\pi/2} = 100$ ns, $t_\pi = 200$ ns, $\tau = 460$ ns. The arrow shows the position at which the ENDOR measurements were carried out.

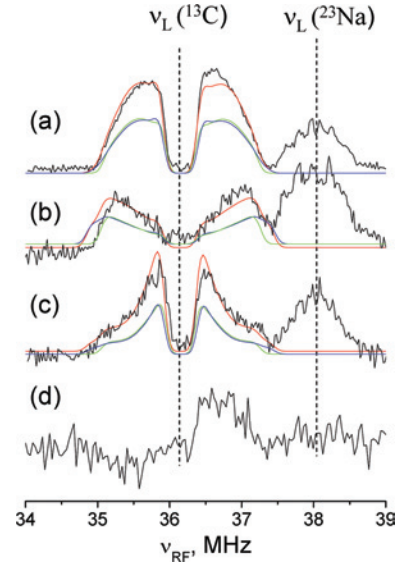

Figure 4. ENDOR spectra of the Mn^{2+}−bicarbonate complex ([Mn] = 0.5 mM and $[NaHCO_3] = 500$ mM). Thick traces are the experimental spectra and the thin traces are simulations of the contributions of the individual nuclei and their sum with a 1:1 ratio, obtained with parameters listed in the text. (a) Mims ENDOR recorded with $\tau = 350$ ns and $t_{\pi/2} = 16$ ns; (b) Davies ENDOR, inversion pulse $t_\pi = 300$ ns and echo detection pulses of $t_{\pi/2} = 150$ ns and $t_\pi = 300$ ns; (c) Davies ENDOR, inversion pulse $t_\pi = 1$ μs, detection via FID following $t_{\pi/2} = 500$ ns; and (d) variable mixing time Mims ENDOR with t_{mix} of 0.5 ms and other parameters as in (b).

(18) Stoll, S.; Schweiger, A. *J. Magn. Reson.* **2006**, *178*, 42–55.
(19) Mims, W. B *Proc. R. Soc. Ser. A—Math. Phys. Sci.* 1965, *283*, 452.
(20) Höfer, P. Ph.D. Thesis, Physikalisches Institut der Universitat, Stuttgart, 1988.
(21) *Gaussian 98, Revision A.11wis, with B97-n/HCTH-npatch*; Frisch, M. J.; Truck, G. W.; Schlegel, H. B.; Scuseria, G. E.; Robb, M. A.; Cheeseman, J. R.; Zakrzewski, V. G.; Montgomery, Jr., J. A.; Stratmann, R. E.; Burant, J. C.; Dapprich, S. Millam, J. M.; Daniels, A. D.; Kudin, K. N.; Strain, M. C.; Farkas, O.; Tomasi, J.; Barone, V.; Cossi, M.; Cammi, R.; Mennucci, B.; Pomelli, C.; Adamo, C.; Clifford, S.; Ochterski, J.; Petersson, G. A.; Ayala, P. Y.; Cui, Q.; Morokuma, K.; Salvador, P.; Dannenberg, J. J.; Malick, D. K.; Rabuck, A. D.; Raghavachari, K.; Foresman, J. B.; Cioslowski, J.; Ortiz, J. V. Baboul, A. G.; Stefanov, B. B.; Liu, G.; Liashenko, A.; Piskorz, P.; Komaromi, I.; Gomperts, R.; Martin, R. L.; Fox, D. J.; Keith, T.; Al-Laham, M. A.; Peng, C. Y.; Nanayakkara, A.; Challacombe, M.; Gill, P. M. W.; Johnson, B.; Chen, W.; Wong, M. W.; Andres, J. L.; Gonzalez, C. Head-Gordon, M.; Replogle, E. S.; Pople, J. A. Gaussian, Inc.: Pittsburgh, PA, 2001.
(22) Neese, F. *ORCA, an ab initio density functional and semiempirical program package*; University of Bonn: Bonn, Germany, 2007.
(23) Schäfer, A.; Horn, H.; Ahlrichs, R. *J. Chem. Phys.* **1992**, *97*, 2571–2577.
(24) Neese, F. *Inorg. Chim. Acta* **2002**, *337*, 181–192.
(25) Wachters, A. J. H. *J. Chem. Phys.* **1970**, *52*, 1033–1036.
(26) Reed, G. H.; Markham, G. D. *Biol Magn Reson.* **1984**, *6*, 73142.

dominated by signals arising from the $M_S = \pm 1/2$ manifold.[11] Signals corresponding to $M_S \neq \pm 1/2$ manifolds should, in principle, appear as well but their intensity is weaker and they are broader by a factor of $|2M_S|$[27] (see eq 4).

The W-band Mims ENDOR (Figure 4a) exhibits a doublet of lines centered about the ^{13}C Larmor frequency ($\nu_L(^{13}C) = 35.9$ MHz) and a second group of lines centered about the ^{23}Na Larmor frequency ($\nu_L(^{23}Na) = 37.8$ MHz). While both Mims and Davies ENDOR spectra suffer from blind spots for small couplings, the spectral shape of the "blind" region is different in each of the experiments. Therefore, recording the ENDOR spectra under conditions that yield different suppression behavior allows determining small hyperfine couplings more uniquely. Accordingly, we recorded three spectra, shown in Figure 4, (a) regular Mims ENDOR with $\tau = 350$ ns; (b) echo-detected Davies ENDOR with an inversion pulse of 300 ns, and (c) FID-detected Davies ENDOR (sequence in Figure 2c) with inversion pulse of 1 μs (Figure 4). These experiments represent the following three limiting situations, respectively: (1) optimum ENDOR effect in Mims ENDOR (Figure 4a), (2) ENDOR lines lying within the suppression hole in Davies ENDOR (Figure 4b), and (3) the smallest possible suppression hole in Davies ENDOR (Figure 4c). Here the duration of inversion pulse is close to the phase memory time of the sample, 1.3 μs, and therefore an echo detection for the Davies ENDOR becomes highly inefficient and an FID detection is a better alternative in terms of signal-to-noise ratio. Simulations of the ENDOR spectra recorded under those significantly different conditions with the same set of hyperfine parameters are expected to give more unique values than those obtained from only one of them.

The three ENDOR spectra could be best fitted with a model having two slightly inequivalent ^{13}C nuclei (1:1 ratio) with isotropic and anisotropic hyperfine couplings: $A_{iso1} = 1.2$ MHz, $T_{1\perp} = 0.7$ MHz, $A_{iso2} = 1.0$ MHz, $T_{2\perp} = 0.6$ MHz, as shown in Figure 4a−c. The simulations show that a slight deviation from axiality of ~0.1 MHz for both types cannot be excluded. Using the point-dipole approximation and neglecting spin densities on the ^{17}O and ^{13}C atoms, the above $T_\perp$ values yield Mn−C distances of 3.05 and 3.2 Å, respectively. To verify the sign of the ^{13}C hyperfine splitting, we applied the VMT Mims ENDOR sequence (Figure 2d) experiment with a mixing time of 0.5 ms. During the long mixing period, ENDOR signals belonging to the $M_S = 1/2$ manifold decay faster than those from the $M_S = -1/2$ manifold, and therefore they can be identified.[14,15] The VMT spectrum shown in Figure 4d has a signal at $\sim\nu^{13}C + 0.5$ MHz, and hence, according to eq 4, the sign of the hyperfine coupling is positive.

The application of the VMT ENDOR experiment has been explained and demonstrated only for spin $1/2$.[14,15] However, the main conclusions should hold also for the case of higher spins. Indeed, in the approximation that cross-relaxation and nuclear relaxation times are much longer than the longitudinal

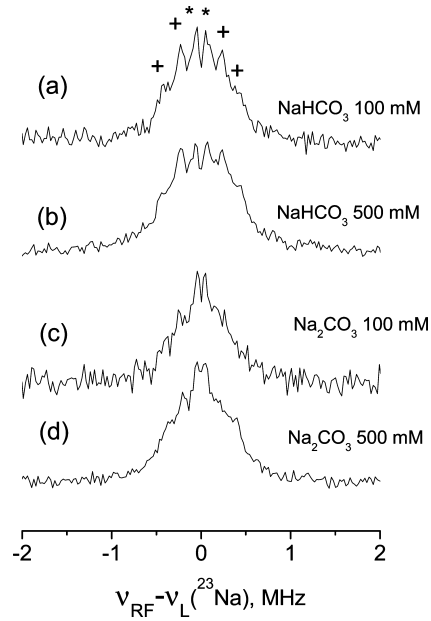

Figure 5. Mims ENDOR spectra of Mn^{2+} with natural abundance bicarbonate and carbonate complexes in the solution. The asterisks (*) and pluses (+) designate the spectral features belonging to distant and close nuclei, respectively. Experimental conditions: $t_{\pi/2} = 16$ ns, $\tau = 350$ ns, $t_{rf} = 30$ μs.

one the equilibrium populations for α and β nuclear states are reached independently. That is, if a RF pulse creates excess amount of α-spins, this excess will be spread over all the electron levels by electron relaxation, while in each electron level those sublevels corresponding to α-spins will have higher population than the β counterparts. Thus, the presence of additional levels for higher spins may affect only the extent of the asymmetry but will not change the general behavior. In fact, a negative ENDOR effect in Mims ENDOR has been already reported for ^{57}Fe in high-spin Fe(III) ($S = 5/2$), before its origin has been understood.[28]

As mentioned above, another characteristic group of lines is located around $\nu_L(^{23}Na)$. This part of the spectrum shows resolved peaks, uncharacteristic for bulk distant nuclei that usually exhibit a featureless signal at the Larmor frequency. Upon the replacement of $NaHCO_3$ with NaCl (same concentration), the ^{23}Na lines completely disappear. This unambiguously shows that ^{23}Na ions in solution do not contribute to the signal, and all the observed features belong to ^{23}Na associated with the Mn^{2+}−carbonate complex. The intensity of the ^{23}Na line is comparable to that of the ^{13}C line, which means that the sodium nucleus can be found in an appreciable part of the complexes.

Whereas the titration with HCO_3^- does not change to any observable extent the shape of the ^{13}C lines, the relative intensities of different components in ^{23}Na spectrum (marked with * and + in the top of Figure 5a) vary slightly with $[NaHCO_3]$. This is a signature of the contribution to the spectrum of at least two types $^{23}Na^+$ ions with different binding constants. The spectra of the Mn^{2+} complex formed with CO_3^{2-}, also shown in Figure 5, exhibit the same peaks, but those marked with * are more intense than in the HCO_3^- complex. This further supports the presence of two types of $^{23}Na^+$. The features with +, situated at $\nu_{Na} \pm 0.23$ MHz and

(27) Baute, D.; Goldfarb, D. *J. Phys. Chem. A* **2005**, *109*, 7865–7871.
(28) Goldfarb, D.; Strohmaier, K. G.; Vaughan, D. E. W.; Thomann, H.; Poluektov, O.; Schmidt, J. *J. Am. Chem. Soc.* **1996**, *118*, 4665.

ν_{Na} ±0.45 MHz, are assigned to the perpendicular and parallel singularities of powder pattern corresponding the nuclear $^1/_2 \leftrightarrow -^1/_2$ transition. This yields $T_\perp = 0.5$ MHz and using the point dipole approximation a distance of 3.5 Å is obtained. The features marked with * in Figure 5 correspond to a hyperfine coupling of 0.05 MHz and are attributed to $^{23}Na^+$ situated much further away than the first type.

Interestingly, the ^{23}Na ENDOR spectrum does not show a blind spot at Larmor frequency, although there is no contribution from many matrix ^{23}Na nuclei. We attribute this to the presence of nonzero quadrupolar interaction of ^{23}Na. This interaction cannot be observed in the EPR spectra in first order of perturbation theory (for the allowed EPR transitions the m_I of nuclei is conserved) and therefore the presence of quadrupolar couplings does not alter the polarization pattern produced by the preparation pulse in the Davies and Mims ENDOR (eqs 6 and 7). This means that holes corresponding to certain values of hyperfine couplings will persist as in the situation without quadrupolar interaction. While the quadrupole interaction does not affect the EPR line, it does affect the nuclear frequencies; more specifically, it shifts the position of the blind spots in the ENDOR spectrum. Therefore, it modifies the blind spot pattern and may not have a blind spot at ν_L, as observed experimentally for ^{23}Na. The distribution of orientations further smears the blind spot position and it is not observed at all.[29]

Proton-counting experiments based on comparison of the ^{1}H-ENDOR effect should, in principle, give information on the number of water molecules in the first coordination sphere.[30,31] Recent W-band measurements have shown only 15% accuracy for Mn^{2+}, thus making it hard to discriminate between coordination shells differing in only 1 water molecule.[31] For the purpose of water ligand counting, the normalized ^{1}H Davies ENDOR spectra of the Mn^{2+}−bicarbonate complex, a Mn^{2+} aqua complex in 1:1 (by volume) water/methanol solution and a Mn^{2+} aqua complex in H_2O/methanol-d_4 are compared in Figure 6. The strong features at ±0.33 MHz in the spectrum of the Mn^{2+} aqua complex are primarily due to methyl protons of the methanol, since their intensities are considerably reduced upon replacement of methanol by methanol-d_4. We chose the intensity of the ^{1}H ENDOR spectrum at ν_H −4 MHz, which is marked with * in Figure 6, as a measure of number of water ligands because it does not overlap with the signal of any distant protons. The sample prepared in methanol-d_4 has a total of 22.4% less exchangeable ^{1}H nuclei due to the presence of methanol-d_4. Yet, the ENDOR effect of the normal methanol and methanol-d_4 samples at ν_H −4 MHz is the same, setting the accuracy of water ligand counting in our case to ∼20%. Similar measurements performed on Gd^{3+} complexes give better accuracy probably due to subtraction of contributions of nuclear transitions belonging to $M_S \neq \pm^1/_2$ electron manifolds.[30] The coordination of bicarbonate is accompanied by a decrease of 40% in ^{1}H-ENDOR signals at ν_H −4 MHz, confirming the replacement of some of the water ligands by the new carbonate ligand. A change of 33% is expected with the binding of two monodentate carbonates.

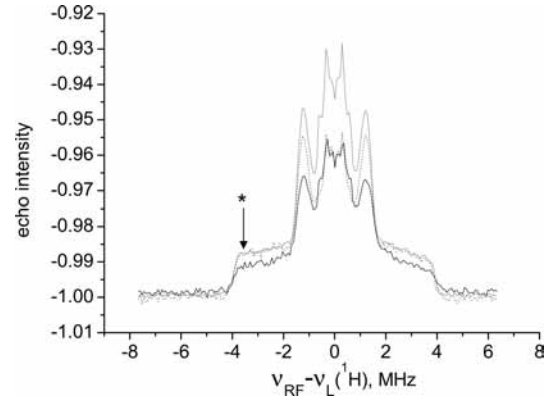

Figure 6. ^{1}H Davies ENDOR spectra of the Mn^{2+} aquo ion in water/methanol solution (gray line), Mn^{2+} aquo ion in water/methanol-d_4 (dotted line), and the Mn^{2+}−bicarbonate complex formed by 0.5 mM [Mn^{2+}] and 250 mM bicarbonate in water/methanol solution (black line). $t_{\pi/2} = 100$ ns $t_\pi = 200$ ns, $t_{rf} = 25$ μs. The asterisk (*) marks the position where the ENDOR effect was evaluated.

Table 1. Summary of the Isotropic Hyperfine Interaction, A_{iso}, the Principal Values of the Anisotropic Hyperfine Interaction [T_{xx}, T_{yy}, T_{zz}] and the Mn−C Distances for the Structures Calculated Using DFT

complex	calculated A_{iso} [T_{xx}, T_{yy}, T_{zz}], MHz	distance, Å
a. one monodentate carbonate	1.15, [−0.76 −0.59 1.35]	3.07
b. two monodentate carbonates I	1.00, [−0.70 −0.56 1.26]	3.17
	1.73, [-0.66 −0.58 1.23]	3.12
c. two monodentate carbonates II	0.91, [−0.70 −0.55 1.25]	3.15
	1.69, [-0.66 −0.58 1.24]	3.12
d. monodentate + bidentate carbonate	1.02, [−0.69 −0.55 1.25]	3.07
	4.60, [-1.13 −0.88 2.01]	2.65
e. one monodentate carbonate + sodium	1.15, [−0.84 −0.65 1.50]	3.05

3.2. DFT Calculations. To substantiate the ENDOR results, DFT calculations were performed. The calculations were carried out on a number of models for monodentate and bidentate coordination modes of bicarbonate without the ^{23}Na ion. The geometry optimization gave a 6-fold coordinated Mn^{2+} in a slightly distorted octahedral geometry. For all monodentate bicarbonates (see Table 1a,b,c, Figure 7) the ^{13}C A_{iso} values are in the range of 0.9−1.7 MHz, which is in good agreement with the experimental value of 1.0−1.2 MHz, and the Mn−C distances are in the range of 3.0−3.2 Å, again in agreement with the experiment. For bidentate bicarbonate coordination, only one complex was found (Figure 7d). For all other possible bidentate models, the geometry optimization converged to a monodentate bicarbonate. In the bidentate mode Mn−C distance is 2.65 Å and A_{iso} =4.6 MHz, which differ significantly from the experimental values. The results of the DFT calculations are summarized in Table 1. The anisotropic hyperfine interaction deviates slightly from axiality (10−15%), and it is attributed to the small spin density on the oxygen (see Table 1). The values of T_{xx} and T_{yy} are quite close to the experimental value of $T_{1\perp}$ and $T_{2\perp}$ (0.7 and 0.6 MHz, respectively).

(29) Walsby, C.; Hong, W.; Broderick, W.; Cheek, J.; Ortillo, D.; Broderick, J.; Hoffman, B. *J. Am. Chem. Soc.* **2002**, *124*, 3143–3151.
(30) Raitsimring, A.; Astashkin, A.; Baute, D.; Goldfarb, D.; Poluektov, O.; Lowe, M.; Zech, S.; Caravan, P. *ChemPhysChem* **2006**, *7*, 1590–1597.
(31) Potapov, A.; Goldfarb, D. *Appl. Magn. Reson* **2006**, *30*, 461–472.

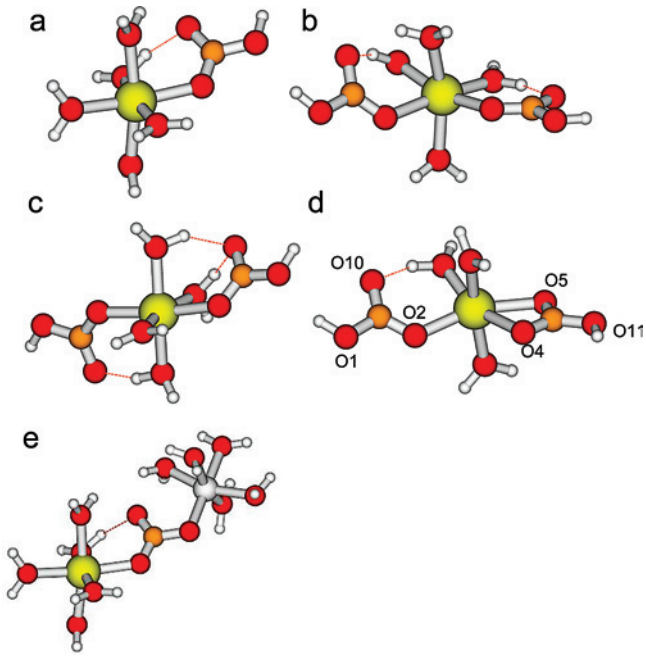

Figure 7. Geometries of model complexes optimized using DFT: (a) one monodentate bicarbonate ligand, (b) two monodentate bicarbonate ligands in neighboring positions (cis), (c) two monodentate bicarbonates ligands, attached to opposite positions (trans), and (d) one monodentate and one bidentate bicarbonate ligands. The oxygen labeling corresponds to those used in Table 2. (e) Same as (a) with a Na^+ ion coordinated to one carboxylate oxygen and five water molecules.

Table 2. Mulliken and Loewdin Population Analysis of the DFT Results for Mono- and Bidentate Coordination of Bicarbonate

atom	Mulliken	Loewdin
bidentate bicarbonate		
C	s 0.004400	s 0.003493
	p 0.014028	p 0.009912
O4 (in contact with Mn)	s −0.001078	s 0.004464
	p 0.031323	p 0.038614
O5 (in contact with Mn)	s −0.001355	s 0.004342
	p 0.021167	p 0.027838
O11	s −0.000730	s 0.000177
	p 0.001802	p 0.002675
monodentate bicarbonate		
C	s 0.001915	s 0.000723
	p 0.004578	p 0.002504
O2 (in contact with Mn)	s −0.000682	s 0.004488
	p 0.010636	p 0.019209
O1	s −0.000361	s 0.000137
	p 0.002403	p 0.002249
O10	s 0.000298	s 0.000580
	p 0.000791	p 0.000736

DFT calculations were also performed on a model with a sodium ion (e) to verify that it does not affect significantly the ^{13}C hyperfine parameters. The model is based on the structure (a) with the bicarbonate proton replaced with a sodium ion, coordinated to additional 5 water molecules. The calculation shows no significant variation of hyperfine couplings compared to complex (a).

4. Discussion

The W-band ENDOR measurements have provided the coordination details of the bicarbonate anion to Mn^{2+}. The anisotropic hyperfine interaction was found to be axially symmetric and using the point dipole approximation Mn−^{13}C distances of 3.05−3.20 Å were obtained, in good agreement with the distances DFT calculations provided for the monodentate coordination mode. Additionally, the ^{23}Na observed signals indicate that the Na^+ cations, at least in part of the complexes, are also coordinated to the bicarbonate, which bridges the two metal ions.

The fact that anisotropic hyperfine coupling of ^{13}C is practically axially symmetric means that point dipole approximation is valid and that the neighboring oxygen atoms carry very little of the spin density. This is in agreement with the spin densities obtained by the DFT calculations, listed in Table 2. These do not exceed 0.02 (Mn^{2+} has ∼5) either for bidentate or for monodentate bicarbonate. Similar values of O spin density have been observed previously in hexa-aqua complexes $Mn(H_2{}^{17}O)_6{}^{2+}$ through ^{17}O ENDOR and DFT calculations.[29] This low ^{17}O spin density leads to a small deviation from axiality (10−15%) in the DFT-calculated anisotropic hyperfine interaction, which is beyond experimental accuracy. Assuming a spin density of 0.02 shared between 5 electrons, we can estimate the contribution of spin density localized on O to the hyperfine coupling of ^{13}C as $T' = \rho\gamma_e\gamma_n/r^3 \approx 0.04$ MHz.

Electrochemical titrations have unambiguously shown the formation of $Mn(HCO_3)_2$, a 1:2 complex.[4] In contrast, X-band ESEEM/HYSCORE spectra were analyzed in terms of only one ^{13}C nucleus, assigned to a bidentate carboxylate based on a short Mn−C distance derived from $T_\perp$. The second ligand was not observed in any of the pulsed EPR experiments.[4] The absence of a second ^{13}C nucleus was explained by either a large strain in its hyperfine interaction leading to excessive broadening or to a very small hyperfine interaction. This analysis is inconsistent with the W-band results presented in this work which shows that the carbonate binds as a monodentate ligand. We attribute the inconsistencies to the complications in the analysis of the Mn^{2+} EPR, ESEEM, and HYSCORE spectra recorded at X-band due to the contribution of the ZFS term as discussed in the introduction. In addition, the preceding X-band study, which reported a negative A_{iso} (^{13}C),[4] while our VMT experiment and DFT calculations has determined unambiguously its positive sign. There, however, the sign was not determined directly but was implied from simulations of line shape under the assumption of a point dipole approximation.

To observation that the spectral simulations required at least a couple of ^{13}C nuclei with only slightly different hyperfine couplings suggests that in frozen solution the complex exists in several conformations, differing slightly in binding geometry, and the two sets of values could actually represent a distribution. Alternatively, it could indicate that the two bicarbonate ligands are slightly different. The Mn−C distance estimated from point−dipole approximation is in accord with the results of analysis of crystallographic data performed earlier.[4] As follows from this analysis, the expected Mn−C distance for a monodentate Mn−bicarbonate complex is 3.3−3.35 Å, and for a bidentate one it is 2.75−2.9 Å. The DFT calculated distances and hyperfine couplings also agree better with monodentate bound bicarbonate. Although IR and Raman spectroscopy may resolve the

question of monodentate/bidentate coordination in solution,[32] we could not find the relevant data for Mn^{2+}−bicarbonate complexes in water solution.

The ^{13}C A_{iso} values measured for complexes of Ras·Mn^{2+}·GDP were found to depend on type of amino acid ligand, and they are slightly smaller than those obtained for the Mn^{2+} bicarbonate complex.[3] At the same time, the anisotropic part is almost the same in all cases. There the Mn^{2+} ion is coordinated to the OH group but not to a carboxylate.

Although the ENDOR results show that there maybe two distinct types of ^{13}C nuclei, this does not necessarily provide the total number of coupled nuclei because, in principle, there could be a number of equivalent nuclei. The latter can be determined from the intensity of the ENDOR effect, once a good reference is found.[30,31] Therefore, the conclusion that the Mn^{2+} is coordinated to two monodentate bicarbonate ligands is supported by the electrochemical titrations,[4] the reduction of the ^1H ENDOR effect upon addition of the $NaHCO_3$ solution, and the DFT calculations.

In the above discussion we have not considered the other ligands to the Mn^{2+}, which are most probably water molecules because they are stronger ligands than the methanol molecules present in large extent. However, the results of ^1H-ENDOR spectrum show a significant reduction in the methyl protons line intensity upon binding of bicarbonate. This suggests that some methanol is present in either first or second coordination shell and is replaced by the bicarbonate.

An interesting finding is the observation of the ENDOR signal of ^{23}Na ion in the complex, showing that carbonate ion bridges two positive ions. This, however, is not surprising because the dissociation constant of the $NaHCO_3$ complex, as determined by electrochemical titrations,[34] is 0.677 M^{-1}. Neglecting the activity coefficients, this estimates 30% of nondissociated complexes in solutions of 500 mM $NaHCO_3$ and ∼10% for 100 mM, consistent with our observation. This implies that using ENDOR it may be possible to detect bridging carboxylates also in proteins, such as concanavaline A where Asp10 is coordinated to both Mn^{2+} and Ca^{2+}.[33]

5. Conclusions

Davies and Mims W-band ^{13}C-ENDOR measurements, corroborated with DFT calculations, showed that in a water/methanol solution Mn^{2+} is coordinated to two monodentate bicarbonate/carbonate ligands. Moreover, the carbonate was found, at least in part of the complexes, to coordinate also Na^+ and it acts as a bridging ligand. This observation suggests that Mn^{2+} maybe be used in the future as a probe for Na^+ binding in systems involving high concentration of negatively charged groups such as in nucleic acids.

In addition, this study demonstrates the resolving power of W-band ENDOR and its simplicity as compared to X-band for the characterization of the coordination shell of Mn^{2+}. Moreover, it shows that for small hyperfine couplings the suppression effect of pulse the ENDOR measurements has to be taken into account and several measurements under different conditions have to be carried out to obtain a unique analysis of the spectra.

Acknowledgment. This research has been supported by Israel Science Foundation (ISF). D.G. holds the Erich Klieger Professorial Chair in Chemical Physics.

Supporting Information Available: Calculation of the shape of the suppression hole in FID-detected Davies ENDOR and its dependence on the width of the detection window. This material is available free of charge via the Internet at http://pubs.acs.org.

IC8011316

(32) Palmer, D. A.; Van Eldik, R. *Chem. Rev.* **1983**, *83*, 651–731.

(33) Deacon, A.; Gleichmann, T.; Kalb, A. J.; Price, H.; Raftery, J.; Bradbrook, G.; Yariv, J.; Helliwell, J. R. *J. Chem. Soc., Faraday Trans.* **1997**, *93*, 4305–4312.

(34) Nakayama, F. S. *J. Phys. Chem.* **1970**, *74*, 2726–2728.